Glass transition in pure and doped amorphous solid water: An ultrafast microcalorimetry study

M. Chonde, M. Brindza, and Vlad Sadtchenko[a)]
Department of Chemistry, The George Washington University, Washington, DC 20052

(Received 27 March 2006; accepted 28 July 2006; published online 1 September 2006)

Using an ultrafast scanning microcalorimetry apparatus capable of heating rates in excess of 10^5 K/s, we have conducted the first direct measurements of thermodynamic properties of pure and doped amorphous solid water (also referred to as low density amorphous ice) in the temperature range from 120 to 230 K. Ultrafast microcalorimetry experiments show that the heat capacity of pure amorphous solid water (ASW) remains indistinguishable from that of crystalline ice during rapid heating up to a temperature of 205±5 K where the ASW undergoes rapid crystallization. Based on these observations, we conclude that the enthalpy relaxation time in pure ASW must be greater than 10^{-5} s at 205 K. We argue that this result contradicts the assignment of glass transition temperature to 135 K and that ASW may undergo fragile to strong transition at temperatures greater than 205 K. Unlike pure ASW, we observe an approximately twofold rise in heat capacity of CH_3COOH doped ASW at 177±5 K. We discuss results of past studies taking into account possible influence of impurities and confinement on physical properties of ASW. © *2006 American Institute of Physics*. [DOI: 10.1063/1.2338524]

I. INTRODUCTION

Water is an unusual liquid which structure and properties are not well understood in spite of centuries of scientific inquiry. The anomalous properties of water are manifested most noticeably when it is supercooled below the equilibrium freezing point near 273 K. For example, constant-pressure specific heat capacity, coefficient of thermal expansion, and isothermal compressibility of water begin to diverge (increase dramatically) as temperature approaches 228 K (T_s).[1] Over the past decades, there have been numerous theoretical attempts to provide a consistent physical picture of structural and dynamic properties of water under various conditions. For instance, the rapid increase in the heat capacity of supercooled water near T_s is explained by the stability limit hypothesis, which postulates the existence of a thermodynamic singularity point near 228 K.[1,2] An alternative explanation is provided by a singularity-free percolation hypothesis, which predicts a rapid rise but not a true discontinuity in thermodynamic functions at this temperature.[1,3] Recently, Mishima and Stanley[1] proposed the existence of a liquid-liquid phase transition to explain the rapid change in thermodynamic functions near T_s. Although this hypothesis postulates a critical point on water phase diagram at P_c = 100 MPa and T_c = 220 K, at pressures below the critical it predicts a λ-like continuous dependence of heat capacity near T_s.

One of the goals of theoretical and experimental research into structure and dynamics of condensed aqueous phases is to provide insights into relationships between various noncrystalline forms of H_2O, i.e., liquid, supercooled, and glassy (amorphous). The amorphous states of water exist at temperatures below the glass transition temperature T_g, and while remaining as static as crystalline phases they are characterized by the lack of long-range molecular order. A well-known example of such a phase is low density amorphous ice,[4] which is the primary focus of this article. Before proceeding, we note a slight terminology disagreement with respect to amorphous water phases prepared by different techniques. While "low density amorphous (LDA) ice" and "amorphous solid water" are often used interchangeably by some investigators, others note that LDA *ice* is a misnomer and low density amorphous solid water (ASW) should be used to designate amorphous water phase, especially, when the samples are prepared by vapor deposition. In line with the recent tradition, we will use ASW as the term for low density amorphous ice in this article.

Development of realistic models of structural and dynamic transformations in water upon supercooling requires measurements of its properties (diffusivity, viscosity, heat capacity, etc.) at temperatures near and below T_s. However, such measurements have proven to be a great experimental challenge. Typically, glasses are formed by rapid cooling of a liquid. While pure water samples usually freeze at temperatures significantly below 0 °C, water is not a good glass former. Unless the cooling rate is exceedingly high (10^7 K/s) and the sample dimensions are microscopic, crystallization becomes nearly inevitable as the temperature of supercooled water is lowered to the vicinity of T_s.[5,6] Indeed, there are only a few experiments conducted under rather extreme conditions where supercooling of water below T_s was reported. For example, Bartell and co-workers have determined that nanoscale water clusters produced by supersonic expansion in vacuum freeze into cubic ice at temperatures as low as 200 K.[7–9] Although the molecular beam approach made it possible to generate liquidlike H_2O cluster with tem-

[a)]Author to whom correspondence should be addressed. Electronic mail: vlad@gwu.edu

perature significantly below T_s, the nanoscale dimensions, extremely short time scale, and a likely presence of large thermal gradients make measurements of thermodynamic properties of supercooled water under these experimental conditions virtually impossible.

The alternative approach to measurements of properties of supercooled water utilizes glassy water samples grown either by slow H_2O vapor deposition[4] or by hyperquenching of microscopic water droplets and clusters on a substrate maintained at cryogenic temperatures.[5,6] After preparation, an amorphous sample's temperature can be gradually increased, and its heat capacity can be measured by differential scanning calorimetry (DSC). In particular, Mayer and coworkers have used this approach to search for a glass transition in ASW.[10,11] In a conceptually similar type of experiment, the self-diffusivity in thin (30–50 nm) vapor-deposited amorphous solid water films was measured in temperature programed desorption (TPD) experiments by Smith *et al.*.[12] Although this approach makes it possible to obtain significant insights into properties of glassy water, it is limited to a relatively narrow temperature range. As the temperature of an ASW sample is raised above 160 K, ASW rapidly crystallizes to cubic ice.[4] Thus, the characteristic temperature of rapid ASW crystallization ($T_c \geqslant 160$ K) and the temperature of catastrophic freezing of supercooled water ($T_s \sim 228$ K) mark the borders of a temperature region, dubbed as *No Man's Land*, where experimental studies of noncrystalline states of water seem to be impossible.[1]

While T_s may be a thermodynamic singularity point, the characteristic temperature of ASW crystallization certainly does *not* represent any true phase transition temperature. Like supercooled water, ASW is metastable with respect to crystalline phase with crystallization rate constant governed by an Arrhenius dependence on temperature.[13,14] Consequently, the T_c simply represents a characteristic temperature at which the crystallization rate of ASW becomes significantly high so that the time required for complete conversion of an ASW sample to a crystalline form is shorter than the typical time scale of a DSC or TPD experiment (20–200 s). This leads to an important conclusion: At least the lower boundary of the No Man's Land region is defined by capabilities of the experimental setup (the heating rate of the DSC or TPD instrumentation). Therefore, the temperature range of experimental studies of ASW properties can be extended with a custom-made instrument, which is capable of thermodynamic or kinetic measurements during rapid heating before a significant fraction of the ASW sample has crystallized.

With the objective of gaining insights into properties of deeply supercooled water at temperatures in the No Man's Land region, we recently developed an ultrafast microcalorimetry apparatus. In our experiments thin 1–3 μm thick films of ASW are prepared by H_2O vapor deposition on the surface of a thin (10 μm in diameter) tungsten filament at cryogenic temperatures in vacuum. The films are then heated with rates up to 10^5 K/s by passing an electrical current pulse through the filament. During this rapid heating, the filament acts as the heater, the temperature sensor, and the sample holder facilitating heat capacity measurements of the ASW films in a manner similar to a basic scanning calorimetry experiment. Nevertheless, the high heating rates make it possible to conduct studies of thermodynamic properties and phase of ASW at temperatures as high as 205 K. In this article, we report the results of our first investigation into properties of ASW in the No Man's Land.

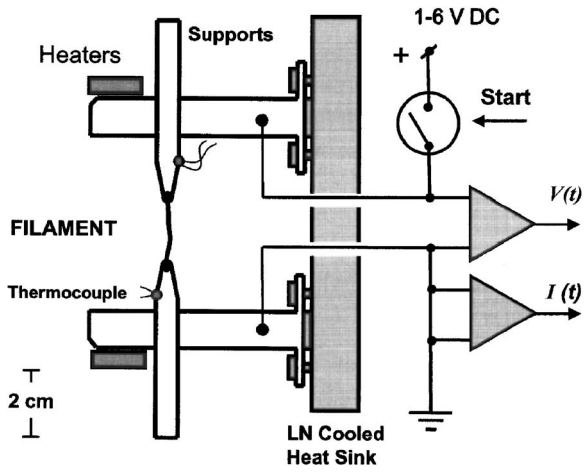

FIG. 1. Outline of the ultrafast microcalorimeter. The microcalorimeter is essentially a thin tungsten filament of 10 μm in diameter and 2 cm long. The filament is spot-welded to two supports in thermal contact with liquid nitrogen (LN)-cooled heat sink through 1 mm thick sapphire plates. While providing a moderate thermal contact with the heat sink, the sapphire plates ensured that the filament and the supports are electrically isolated from the rest of the apparatus. Two resistive heaters capable of dissipating up to 10 W of power are attached to the filament supports. During vapor deposition of ASW films, the temperature of the filament could be varied from 120 to 170 K through balancing of the heat load from the resistive heaters against thermal conductance to the LN-cooled heat sink through sapphire plates. The temperature of the filament supports during film deposition is monitored with two miniature thermocouples (T type). Rapid heating of the filament is triggered by a pulse from a PC based data acquisition system. During rapid heating, the voltage drop across the filament and the current through the filament are recorded every 4 μs.

II. EXPERIMENT

Experiments were conducted using a custom-designed ultrafast microcalorimeter, which is the central part of our novel apparatus for time-of-flight and thermal desorption spectroscopy studies of reactions and dynamics in thin aqueous films. The apparatus is equipped with a sensitive doubly differentially pumped quadrupole mass spectrometer and in addition to analysis of chemical composition of aqueous films makes it possible to conduct time-of-flight (TOF) studies of velocity distribution of chemical species desorbing from the filament during rapid heating. A full description of components of this instrument is given elsewhere.[15] Therefore, we will focus primarily on the microcalorimeter design.

As shown in Fig. 1, the microcalorimeter is essentially a thin tungsten filament of 10 μm in diameter and 2 cm long (Goodfellow). The filament was spot-welded to two supports in thermal contact with liquid nitrogen (LN)-cooled heat sink through 1 mm thick sapphire plates. While providing a moderate thermal contact with the heat sink, the sapphire plates ensured that the filament and the supports are electrically isolated from the rest of the apparatus. Two resistive heaters capable of dissipating up to 10 W of power were attached to

the filament supports. During vapor deposition of ASW films, the temperature of the filament could be varied from 120 to 170 K by balancing of the heat load from the resistive heaters against thermal conductance to the LN-cooled heat sink through sapphire plates. The temperature of the filament supports during film deposition was monitored with two miniature thermocouples (T type).

The vapor deposition system for the preparation of ASW films consisted of 12 effusive dosers and the vapor source. The dosers were 1/8 in. in diameter stainless steel tubes equally spaced around the filament at the distance of about 5 cm from its center (not shown in the figure). Each tube was positioned at the angle of about 60° with respect to the filament axis. The vapor deposition system was capable of sample growth rates from 1 to 50 ice ML/s. The dosing time was between 5 and 300 s. De-ionized H_2O was degassed before use each day. The microcalorimeter assembly with the effusive dosers was surrounded by six cryogenic shields and positioned inside a vacuum chamber pumped with a 2500 l-s^{-1} Varian diffusion pump. During all experiments, the chamber was maintained at the base pressure of 3×10^{-7} Torr.

After deposition of an ASW film, rapid heating of the filament was triggered by a pulse from a personal computer (PC) based data acquisition system. The activation time was less than 1 μs. The trigger pulse closed an electronic switch connecting the filament assembly to the positive output of a dc power supply (Sorceren) set at 3–5 V. While maintaining the constant voltage, the power supply allowed free variation in the filament current. During rapid heating a set of two values, voltage drop across the filament and the current through the filament, was recorded every 4 μs.

Results of a typical microcalorimetry experiments are summarized in Fig. 2. The solid line shows resistance of a filament covered by a micrometer thick amorphous ice film. The resistance of an ice-free filament is shown for comparison. The effective resistance values were calculated from current and voltage data according to Ohm's law. The temperature was calculated from the resistance data using the following equation:

$$T(R) = T_0 - (1/\alpha)(1 - R/R_0), \quad (1)$$

where α is the temperature coefficient of electrical resistivity of tungsten (0.0045 °C^{-1}). As it follows from Eq. (1), derivation of the temperature values from the filament resistance data relies on accurate measurements of the effective resistance of the filament R_0 at a known temperature T_0. Thus, a three-point calibration procedure was developed in order to improve the accuracy of the resistance based temperature measurements in our experiments. First, resistance of the filament was measured when the microcalorimeter assembly was cooled down to near LN temperature, i.e., at T_0(cryogenic)=120±1 K. The value of T_0 (cryogenic) was assumed to be equal to that measured with two thermocouples attached to the filament supports. Second, the filament resistance was measured when the microcalorimeter assembly was warmed up to ambient temperature, i.e., at T_0(ambient)=303±1 K. Once again, the value of T_0 (ambient) was assumed to be equal to that measured with the thermocouples. Third, as described in our previous article, a steady-state resistance value was recorded during a thermal desorption spectroscopy (TDS) experiments where fully crystallized ice films underwent melting at T_0(melting) =273±1 K.[15] Finally, the accuracy of resistance based temperature measurements was verified between 220 and 270 K by time-of-flight analysis of the flux of water molecules desorbing from ice surface.[15] Using this extensive calibration procedure made it possible to reduce the temperature measurement errors to ±1.5 K.

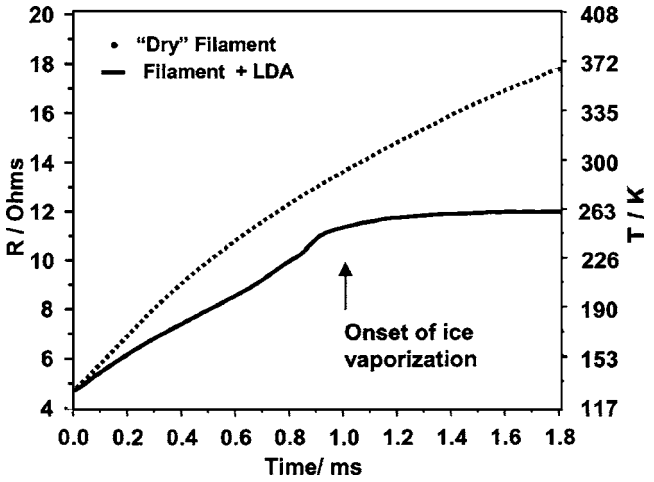

FIG. 2. Resistance and corresponding temperature of the filament during rapid heating. The solid line shows resistance of the filament covered by a micrometer thick amorphous ice film. The resistance of an ice-free filament is shown for comparison. The effective resistance values were calculated from the current and voltage data according to Ohm's law. The temperature was calculated from the resistance data using the temperature coefficient of electrical resistivity of tungsten. In the case of the ice-covered filament, the heating rate is lower, and the heating curve shows a number of inflection points indicative of multiple exo- or endothermic transitions in the filament-ice system. The data demonstrate that heating rates up to 10^5 K/s are easily accessible with the experimental setup and that the sensitivity of the microcalorimeter is sufficient to detect exo- and endothermic transitions in thin films of amorphous ice used in our experiments.

As shown in Fig. 2, applying a small (3.4 V) potential across the filament results in a rapid temperature rise of ice-free and ice-covered filaments. However, in the latter case, the heating rate is significantly lower signifying greater thermal mass of the ice-covered filament. Furthermore, the heating curve is complex and shows a number of inflection points indicative of multiple exothermal transitions in the filament-ice system. In short, Fig. 2 demonstrates that heating rates on the order of 10^5 K/s are easily accessible with the experimental setup and that the sensitivity of the microcalorimeter is sufficient to detect exo- and endothermic transitions in thin films of amorphous ice used in our experiments.

As shown in Fig. 2, the rapid rise in temperature during the first milliseconds of the experiment is followed by a region where the temperature of the ice-filament system is nearly constant ($\Delta T < 1$ K). As described in our previous article,[15] this is due to the onset of rapid vaporization of the ice film which follows zero-order kinetics. Based on our vaporization rate studies, we conclude that ice films grown under conditions present in our experiments have neat cylindrical geometry and cover the filament surface completely.

Furthermore, the time-of-flight analysis of the velocity distribution in the flux of desorbing water along with the kinetics of vaporization indicate that longitudinal and transverse temperature gradients in micrometer scale ice films are less 1–2 K during steady-state vaporization regime. Although the temperature gradients may be somewhat greater during initial temperature rise, we note that according to our extensive heat transfer calculations these cannot exceed a few degrees even for the aqueous films with low (waterlike) thermal conductivity. We discuss possible thermal gradients and lags in greater detail in the next sections of this article.

III. RESULTS AND DISCUSSION

A. Ultrafast microcalorimetry of toluene

To our knowledge ultrafast scanning microcalorimetry has never been used to study ASW. Because of the lack of reliable data on dynamic and thermodynamic properties of this aqueous solid, we will first demonstrate the viability of our experimental approach using a system which is well understood. An excellent example of such a solid is a vitreous state of toluene. Unlike DSC experiments with ASW, which results are currently contested,[16,17] DSC thermograms of glassy toluene show a well defined (near twofold increase in heat capacity) glass transition at 117.5 K.[18] Furthermore, there is a wealth of data on relaxation time in toluene covering the entire temperature range from cryogenic to ambient while there are only a few such measurements in the case of ASW.[19]

In our experiments with toluene, 0.2–2 μm thick films were deposited on the filament at 110 K. After deposition, the films were annealed by warming the calorimeter assembly to 125 K for a few minutes to allow the highly strained vapor-deposited structure to release the excess enthalpy and to ensure collapse of likely pores in its bulk. After annealing the temperature of the microcalorimeter was lowered back to 110 K and the rapid heating of the filament was initiated. Similar to H_2O ice films, the toluene samples showed zero-order desorption kinetics following the initial temperature rise. Zero-order desorption kinetics indicated that toluene was deposited in the form of a uniform multilayer film which covered the entire surface of the filament.[15]

Figure 3 shows the thermogram of 0.8 μm thick amorphous toluene film. The heating rate was $(1.3\pm0.2)\times10^5$ K/s. A well-pronounced upswing in heat capacity characteristic of the glass transition is at 135 K. The twofold increase in the heat capacity observed during ultrafast calorimetry scan is consistent with the heat capacity rise from 80 to 150 J/mol K observed in conventional DSC studies.[18] Nevertheless, unlike the glass transition observed in conventional (slow) DSC experiments, the onset of the heat capacity rise occurs at much higher temperature of 135 K during the ultrafast scan. The glass transition during rapid scan is also much broader. The heat capacity rise during ultrafast scan occurs over a temperature interval of 20 K which is significantly greater than a degree wide temperature range characteristic of slow DSC scans. Finally, ultrafast thermogram contains no exothermic features associated with crystallization of amorphous toluene, which demonstrates that it is possible to avoid crystallization of certain amorphous solids when the heating rates are on the kK/s scale.

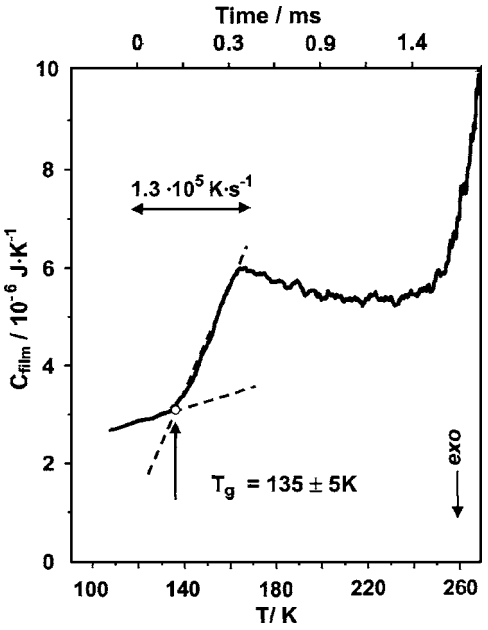

FIG. 3. The thermogram of 0.8 μm thick amorphous toluene film. The film was deposited on the filament at 110 K. After deposition, the film was annealed at 125 K for a few minutes to allow the highly strained vapor-deposited structure to release excess enthalpy. A well-pronounced upswing in heat capacity characteristic of the glass transition is at 135 K. The endothermic upswing in the heat capacity at temperatures above 250 K, present in all thermograms, is due to the onset of rapid desorption.

What can we learn from the data in Fig. 3? We begin with assumption that the onset of the glass transition in rapidly heated toluene films is observed at a temperature where the enthalpy relaxation time becomes smaller than the characteristic time scale of our experiment t_{exp} (the enthalpy relaxation time decreases with temperature). We choose the value of 1 K/Q, where Q is the average heating rate, as the measure of t_{exp} and assume then that the enthalpy relaxation time $\tau(T_g)$ is within one order of magnitude of t_{exp} value:

$$\tau(T_g) \approx \frac{10^{\pm0.5}\ \mathrm{K}}{Q}. \tag{2}$$

According to Eq. (2), the heating rate of 1.3×10^5 K/s (typical for our ultrafast experiments) gives the enthalpy relaxation time in the range from 3×10^{-6} to 3×10^{-5} s near 135 K, and the heating rate of 10^{-2} K/s (typical of conventional DSC experiments) gives the relaxation time of approximately 10^2 s near 117 K. As shown in Fig. 4, these values are in excellent agreement with the previous measurements of the relaxation times in toluene.

The analysis described above shows that ultrafast microcalorimetry can be used to determine enthalpy relaxation time at a particular temperature. Moreover, good match between enthalpy relaxation time calculated from ultrafast microcalorimetry data and that obtained in previous experiments indicates that the thermal lags and temperature gradients in the bulk of micrometer scale glassy toluene films have negligible impact on the results of such measurements. In order to further validate this conclusion, we conducted enthalpy relaxation time measurement with vitreous toluene

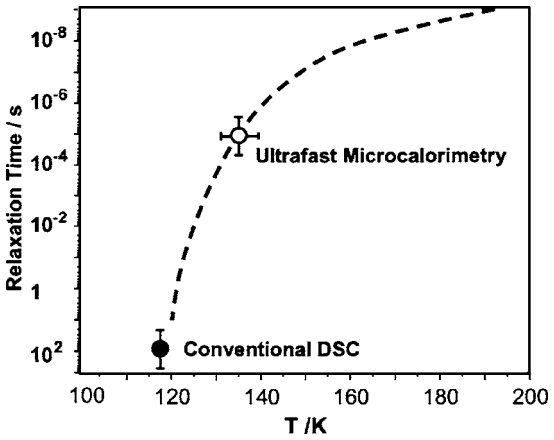

FIG. 4. The enthalpy relaxation time of vitreous toluene at 135 K estimated from the ultrafast microcalorimetry experiments (open circle) and the enthalpy relaxation time at 117 K estimated from conventional DSC studies (solid circle). The dotted line shows compilation of relaxation time data from dielectric spectroscopy, deuteron spin-lattice relaxation, and microwave spectroscopy measurements, as well as measurements of diffusion and viscosity and deuteron spin-alignment experiments (Ref. 19).

films of various thicknesses (from 0.5 to 2 μm). Although we observed small variations in the glass transition temperature (a few kelvins) from scan to scan, these did not correlate with the film's thickness and were most likely due to slight changes in the heating rate (1%–2%) in different experiments and the noise in the thermograms. We conclude, therefore, that the glass transition temperature can be determined in our ultrafast microcalorimetry experiments with the overall accuracy of ±5 K. As we will show in the next sections of this article, this accuracy is sufficient for the essential conclusions of our studies.

B. Ultrafast microcalorimetry of pure and doped ASW

Figure 5 summarizes thermograms of vapor-deposited ice films prepared under various conditions. The mass of the films was nearly identical in all three experiments and corresponded to the ice film thickness of 1.0±0.1 μm. The lower panel shows the thermogram of an ASW film vapor deposited at 110 K. The heating rate was $(1.3\pm0.2)\times10^5$ K/s. The scan reveals three exothermic features marked as A, B, and C at 200, 210, and 220 K, respectively. The middle panel of Fig. 5 shows the thermogram of ASW film vapor deposited at 140 K. While increase in the deposition temperature did not lead to noticeable changes in the magnitude and position of the exothermal B and C peaks, it resulted in complete disappearance of the A peak. Finally, the top panel of Fig. 5 shows the thermogram of a film vapor deposited at 175 K. In this case, the thermogram completely lacks any exothermal features. The endothermic upswing in the heat capacity at temperatures above 250 K, present in all there thermograms, is due to the onset of the rapid desorption.[15]

Taking into account the wealth of data on microstructure and phase transition in vapor-deposited ASW films, the interpretation of the thermograms in Fig. 5 is straightforward. First of all, vapor deposition of water on a cold substrate at temperatures below 120 K results in highly strained and probably microporous ASW. Such a film shows a broad enthalpy relaxation peak in scanning calorimetry experiments at temperatures below onset of crystallization.[17] Noticing that the temperature of the deposition in the second experiment (140 K) is not sufficiently high to result in the extensive crystallization of the film on the time scale of our experiments (120 s), we attribute feature A to the enthalpy release during initial relaxation of microporous ASW film. At the same time, we assign B and C exotherms to film's crystallization. This assignment is consistent with the sensitivity of peak A toward sample deposition rate and temperature observed in our experiments. Indeed, porosity of ASW has been shown to depend strongly on the preparative conditions and thermal history of the sample.[4]

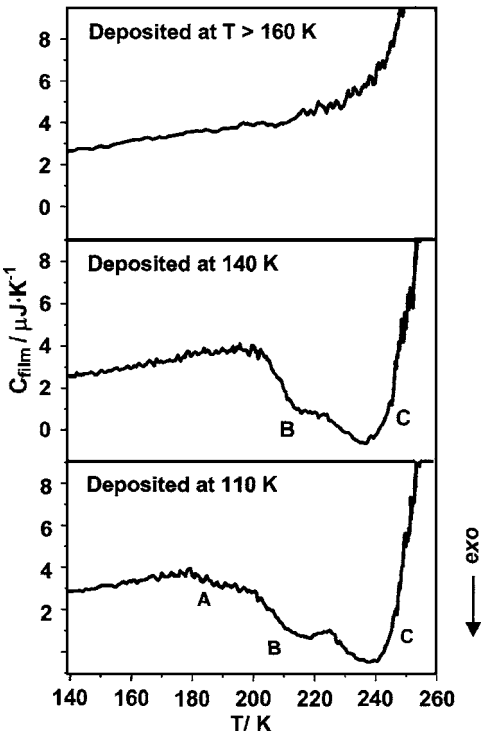

FIG. 5. Ultrafast thermograms of vapor-deposited ice films prepared under various conditions. The heating rate is $(1.3\pm0.2)\times10^5$ K/s. The mass of the films is nearly identical in all three experiments and corresponds to the ice film thickness of 1.0±0.1 μm. Lower panel: the thermogram an ASW film vapor deposited at 110 K. Middle panel: the thermogram of ASW film vapor deposited at 140 K. Top panel: the thermogram of a film deposited at 170 K. The endothermic upswing in the heat capacity at temperatures above 250 K, present in all three thermograms, is due to the onset of the rapid desorption.

Figure 6 compares heat capacities of ASW and crystalline ice films of nearly identical mass. We note that although the accuracy of the absolute measurements of ice sample mass is on the order of 10%, the accuracy of relative measurements was better than 2%. The ASW film's deposition temperature was chosen so that peak A completely disappeared from the thermogram, while exothermic features B and C remained unchanged. In other words, the deposition temperature was sufficiently high to ensure complete relaxation of the strained ASW sample without its extensive crystallization. The most important feature of the thermogram in Fig. 6 is the near match in the heat capacities of the crystalline and the ASW samples up to the temperature of ASW crystallization, i.e., the lack of endothermic features associated with the glass transition. As we will show in the follow-

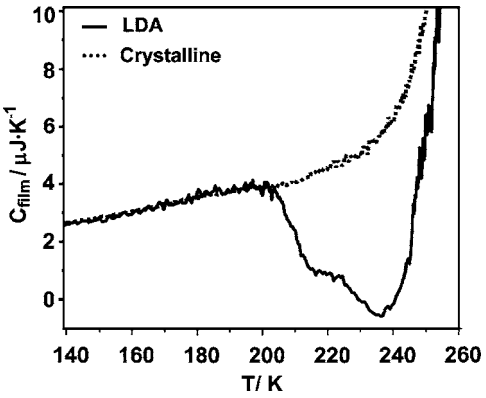

FIG. 6. Heat capacities of ASW (solid line) and crystalline (dots) ice films of nearly identical mass (the accuracy of relative measurements of ice sample mass is better than 3%). The deposition temperature was 140 K and was chosen to ensure complete relaxation of strained ASW sample without its extensive crystallization. The most important feature of the thermogram is the near match in the heat capacities of the crystalline and the ASW samples up to the temperature of ASW crystallization, i.e., the lack of endothermic features associated with the glass transition.

ing sections of this article, this result is in contrast to the assignment of the glass transition temperature to 135 K for ASW.[10]

In order to demonstrate that ultrafast microcalorimetry technique is capable of detecting a glass transition in aqueous systems, we have measured thermograms of ASW samples doped with acetic acid. In these experiments, micrometer thick aqueous films were grown on the filament by codeposition of H_2O and acetic acid vapors at 140 K. The mole fraction of acetic acid in the ASW film was 0.05 ± 0.01 as verified by mass-spectroscopic analysis during the vaporization of the film. Following deposition, the film was cooled to 110 K and the rapid thermal scan was initiated. As shown in Fig. 7 doping of ASW with acetic acid results in an upswing in effective heat capacity of the sample at 177 ± 5 K. Using the same simple analysis as in experiments with toluene, we obtain the value of $(0.3-3) \times 10^{-5}$ s for the enthalpy

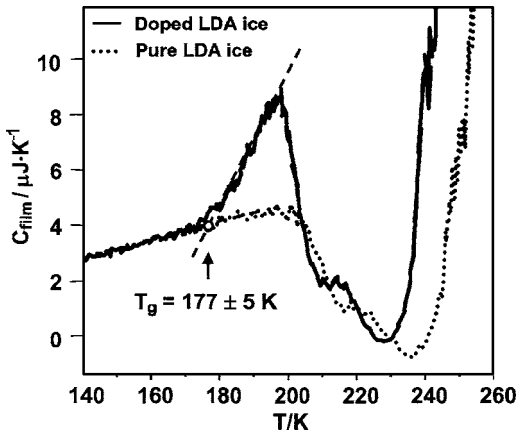

FIG. 7. Ultrafast thermograms of doped (solid line) and pure (dots) ASW samples deposited under near identical conditions. The mole fraction of CH_3COOH in the ASW film was 0.05 ± 0.01 as verified by mass-spectroscopic analysis during the vaporization of the film. Although the glass transition cannot be observed in the case of *pure* ASW, doping of ASW with acetic acid results in characteristic upswing in effective heat capacity of the sample at 177 ± 5 K.

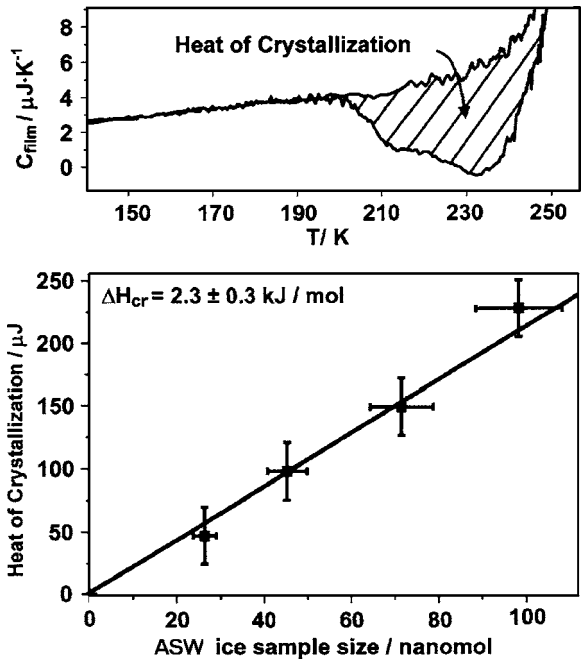

FIG. 8. Top panel: the data analysis for determining the excess heat capacity values from calorimetry scans. The thermogram of crystalline ice sample was used as a base line for subtraction. The excess heat capacity is then integrated to derive the heat of crystallization of ASW in the 200–260 K range. Lower panel: the total heat of crystallization as a function of ice sample size. The resulting enthalpy of ASW crystallization is consistent with the enthalpy release during crystallization of purely amorphous ice samples at cryogenic temperatures.

relaxation time in the H_2O/acetic acid mixture at this temperature. In summary, although the glass transition cannot be observed in experiments with *pure* ASW samples, it is strongly manifested in ASW doped with acetic acid.

C. Glass transition in pure and doped ASW

Before proceeding with interpretation of our results, we must discuss instrumental limitations in our experiments. It can be argued that the lack of an observable glass transition in ultrafast thermograms of pure ice may be due to partial crystallization of the sample, i.e., due to a low ASW content of the sample. Furthermore, the failure to observe the glass transition may be due to temperature lags and gradients present in the micrometer thick ASW films during rapid heating. Finally, the sensitivity of our microcalorimetry setup may not be sufficient to detect the glass transition in ASW. We provide arguments *against* such interpretations of our results immediately below.

First, we emphasize that ice films deposited or annealed at 140 K must consist predominantly of ASW. As illustrated in the top panel of Fig. 8, the excess heat capacity values can be extracted from calorimetry scans using the thermogram of crystalline ice sample as a base line for subtraction and can then be integrated over temperatures to derive the heat of crystallization of ASW in the 200–260 K range. The lower panel of Fig. 8 shows the total heat of crystallization as a function of ice sample size. The resulting enthalpy value of 2.3 ± 0.3 kJ/mole is consistent with the enthalpy release during crystallization of purely amorphous ice samples at cryo-

genic temperatures.[20] Although the heat of crystallization of ASW at temperatures in the 200–260 K range is unknown, it must be lower than that for liquid water (4–5 kJ/mole) and grater than that for low temperature ASW (approximately 2 kJ/mole). Thus, we conclude that the ASW content in our vapor-deposited ice films is *at least* 50%, which is sufficiently high to observe endothermic heat capacity variations in the case of glass softening transition.

Second, in the previous section of this article, we demonstrated that the ultrafast microcalorimetry technique provides reliable detection of the glass transition in vitreous toluene. The enthalpy relaxation time value derived from our measurements is in excellent agreement with results of a multitude of past measurements, including the value obtained in standard DSC studies. Taking into account the fact that the heat conductance of the vitreous toluene films as well as their geometries are similar to those of ASW samples, we conclude that the influence of possible thermal lags and gradients on the relaxation time measurements in our experiments is negligible. This conclusion is further facilitated by experiments with doped ASW samples. While we fail to observe the glass transition in pure ASW samples, it is strongly manifested in samples doped with acetic acid. Because addition of the relatively small amount of impurities to ASW films is not likely to increase their thermal conductivity, the lack of observable glass transition in the case of pure ASW is not due to temperature gradients or thermal lags.

Third, the endothermic features attributed to the glass transition near 136 K in standard DSC experiments with ASW were exceedingly weak.[10,11] Therefore, it can be argued that glass transition is simply below detection limits of our microcalorimetry technique. We emphasize, however, that small variations in heat capacity are characteristic only of low temperatures. If ASW undergoes a glass transition at temperatures near 135 K, the heat capacity of the resulting supercooled liquid must increase rapidly with temperature. For example, according to the theoretical predictions of Johari *et al.*, the heat capacity of supercooled liquid water near 200 K must be at least 50% greater than heat capacity of ASW.[21] Therefore, the glass transition must be detectable at temperatures in the 160–200 K range, even with the typical sensitivity of our apparatus toward variations in sample's heat capacity (3%).

Because instrumental limitations cannot explain the lack of the observable glass transition in our experiments, we argue that the failure to observe glass transition under conditions of ultrafast heating indicates that ASW crystallizes at temperatures lower than those required for glass softening. Seemingly remarkable, this conclusion is in agreement with the hypothesis of Angel and co-workers who argued that the temperature of glass transition in ASW is significantly higher than the temperature of its crystallization, i.e., that the glass transition in ASW is impossible to observe under any experimental conditions.[16,17] Based on the analysis of the thermograms of a variety of high enthalpy glasses, they concluded that the temperature of the glass transition for pure ASW should be reassigned from 136 K to a higher value of 165 K, which is within the range of temperatures characteristic of rapid crystallization of amorphous ice. The failure to observe the glass transition in ultrafast microcalorimetry studies provides further support for this hypothesis and indicates that glass softening of ASW is much slower than crystallization at temperatures up to 205 K.

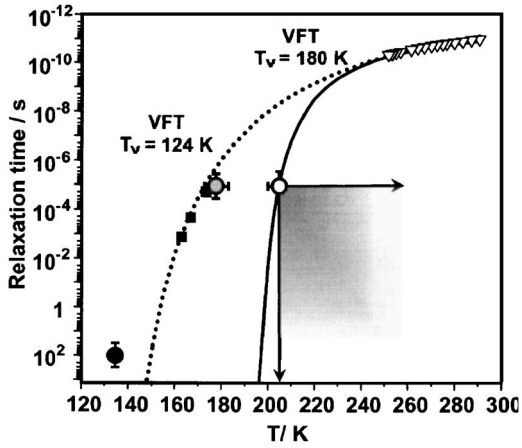

FIG. 9. The relaxation time data from various experiments. Solid circle at 135 K: the enthalpy relaxation time estimated from conventional DSC studies assuming that the observed weak endothermic feature was, in fact, a glass transition. Solid squares: the dielectric relaxation times obtained in experiments with poly(HEME) matrix soaked in water. Grey circle at 177 K: the enthalpy relaxation time obtained in our ultrafast microcalorimetry experiments with ASW doped with acetic acid. Open circle at 250 K: the *minimum* possible enthalpy relaxation time estimated from our experiments with pure ASW. Shaded region: the range of possible enthalpy relaxation time values at various temperatures estimated from the results of ultrafast microcalorimetry experiments. Open triangles: the relaxation time data from dielectric spectroscopy experiments with water at ambient temperatures. Dotted line: the VFT fit of the relaxation time data assuming that the Vogel temperature is 124 K. Solid line: the VFT fit of relaxation time data assuming that the Vogel temperature is 180 K. As shown here the enthalpy relaxation times estimated from ultrafast microcalorimetry experiments with pure unconfined ASW are in contrast to the previous measurements. Our data demonstrate that the Vogel temperature for pure unconfined ASW may be as high as 180 K.

Although we do not directly observe glass transition in pure ASW, we can still estimate the *lower limit* for the enthalpy relaxation time at temperature near the onset of crystallization. Because we *do not* observe the upswing in heat capacity below 205±5 K, the enthalpy relaxation time at these temperatures must be *greater* than the time scale of our experiment (10^{-5} s). Alternatively, we can estimate the lowest temperature at which the enthalpy relaxation time becomes comparable to the time scale of our experiment. Because we do not observe the upswing in heat capacity at temperatures below the onset of crystallization, the enthalpy relaxation times must approach the time scale of our experiment at temperatures greater than 205±5 K. Armed with these estimates for the temperature and relaxation time limits, we can revisit some of the arguments in favor of a direct structural and dynamic relationship between ASW at temperatures above 135 K and liquid water at temperatures near ambient.[22,23]

Experimental results often cited in support of the continuity hypothesis include the dielectric spectroscopy study of relaxation in ASW-poly(HEMA) matrix in the 160–175 K temperature range[22] and studies of water self-diffusivity in ultrathin (<30 nm) ASW films between 150 and 160 K.[23] As shown in Fig. 9 (filled squares) the dielectric relaxation time

values can be connected with those measured for liquid water at temperatures above 260 K via the Vogel-Fulcher-Tammann (VFT) equation:

$$\tau = \tau_0 \exp\left(\frac{E_0 T_0}{T_0 - T}\right), \tag{3}$$

where $T_0 = 124$ K is the Vogel temperature, i.e., the temperature of the near complete structural arrest in a glassy system.[22] Thus, according to the argument,[22,23] ASW at temperatures above 124 K can be viewed simply as a deeply supercooled state of liquid water. Smith *et al.* used the water self-diffusivity data near 150 K as an evidence of direct link between ASW and water. Similar to Johari's dielectric relaxation data, their self-diffusivity data resulted in the Vogel temperature of approximately 124 K.[23]

As shown in Fig. 9, our ultrafast microcalorimetry results are in stark contrast with this continuity argument. While, the VFT equation with the Vogel temperature near 124 K fits the enthalpy relaxation time data in the case of *doped* ASW, it fails completely in the case of the pure ASW samples. Indeed, our estimate of the enthalpy relaxation times in the case of pure ASW gives a value grater than 10^{-5} s at 205 K. As illustrated in the Fig. 9, this relaxation time is *three orders of magnitude greater* that that predicted by a VFT fit with the Vogel temperature of 124 K. Although it is still possible that the relaxation times estimated from our microcalorimetry measurements can be linked to the relaxation time data for water with a simple VFT fit, the Vogel temperature of such a fit must be at least 180 K which is significantly higher than the 120–125 K value obtained in dielectric spectroscopy[22] and self-diffusivity[23] experiments. Furthermore, it follows from Fig. 9 that it is impossible to connect the characteristic *enthalpy* relaxation time at 135 K, the enthalpy relaxation time at 205 K, and the relaxation times at temperatures near ambient with a simple VFT equation. Therefore, our results support the notion that the assignment of glass transition temperature to 135 K is *incorrect* and that water, in fact, may *exhibit* anomalous crossover from fragile (above 205 K) to strong liquid (below 205 K).[24,25]

D. Origins of disagreement

The microcalorimetry results described in the previous section are in stark contrast with conclusions of several earlier studies. In this section, we offer a possible explanation for the origins of this disagreement. Our hypothesis is based on the sensitivity of hydrogen bond network to two types of perturbations: confinement and impurities.

There have been experimental and theoretical studies indicating that the physical properties of *crystalline* ice confined to nanoscale dimensions may be different from those of macroscopic samples. For example, under near ambient conditions, termination of hydrogen bond network either at the ice surface or at the interface between ice and another solid leads to extensive liquefaction of the interfacial region even at temperature tens of degrees below normal (bulk) melting point.[25–29] At cryogenic temperatures, the effects of confinement are evident in the vibrational spectra of ice nanoparticles, in which near surface structure may be altered even further by various adsorbates.[30] While the extent of perturbations of the molecular structure of condensed aqueous phase caused by confinement or impurities may not be severe enough to be observed directly, such perturbations may still significantly influence phase transitions and molecular transport. For example, self-diffusion coefficient values for water in *ultrathin* (<100 nm) single crystal ice films appear to be almost two orders of magnitude greater than the values extrapolated from experiments with macroscopic single crystal samples.[31] Furthermore, even micromole concentrations of impurities may result in dramatic changes in the thickness of quasiliquid layers formed at various ice interfaces as the result of interfacial premelting.[32]

Although lacking long-range molecular order, well-annealed, low porosity ASW samples are still characterized by a high extent of tetrahedral coordination of water molecules.[33] In other words, the hydrogen bond network in ASW is highly cohesive with a significant fraction of bulk water molecules in a fully associated state. Therefore, it is possible that confinement and impurities play important role not only in the cased of crystalline but also in the case of amorphous ice.[34] For example, severe perturbation to this amorphous hydrogen bond network caused by impurities in the ASW matrix or by vicinity of an interface may have a dramatic effect on the molecular kinetics at temperatures below 160 K, i.e., near the hypothesized glass transition in ASW. Indeed, as reported in this article, doping the ASW samples with a relatively small amount of acetic acid results in a heat capacity jump near 177 K, which is not observed for pure ice samples.

We note that current theoretical discussion on properties of ASW is focused on the impurity-free bulk aqueous phases and not on the water in confining geometry or amorphous solid solutions. Therefore, in our microcalorimetry experiments, we attempted to minimize the possible influence of impurities and confinement on the results of our studies. As we have already described, meticulous mass-spectroscopic analysis shows that our ASW samples grown in high vacuum by vapor deposition contain less than ppm concentrations of impurities. Furthermore, we emphasize that physical properties of our *micrometer* thick ASW films grown on a filament with a diameter of 10 μm are *unlikely* to manifest significant confinement effects. While the ultrafast microcalorimetry studies described in this article were conducted with relatively pure ASW samples of *near-macroscopic* dimensions, the same is not true for many of the previous studies. Thus, we argue that confinement effects and the presence of impurities in the ASW samples used in the past experiments are the main sources of the discord between our and previous measurements.

Taking into account the possibility of dramatic changes in ASW properties due to impurities and confinement, we question the relevance of some of the past experimental results to glass transition phenomena in pure unconfined ASW. First, we note that the dielectric relaxation time values from Ref. 22 (filled squares in Fig. 9) were not obtained in experiments with ASW samples. In fact, these studies were conducted with poly(HEMA) matrix, which was "swollen" in

water for several weeks. We also note that many characteristics of this system such as the morphology of the polymer matrix and its precise chemical composition were unknown, except for the water content (58% by mass). Although an attempt was made to gauge the influence of the poly(HEME) on the results of the measurements, we note that the experiments relied on changes in the dielectric relaxation times due to variations in water content in a narrow range (from 58% to 21%). Therefore, the extrapolation of these results to the case of pure water may be invalid.

We also argue that measurements of water self-diffusivity in thin ice films[23] must be interpreted with caution. We point out that these studies were conducted with exceedingly thin amorphous ice film (approximately 10 nm or 30 ice ML) at temperatures consistent with crystallization of the amorphous phase. Because crystallization may lead to fracturing of thin films, self-diffusivity studies in the 145–160 K may be influenced by interfacial transport along the ruptures and related defects in the film's bulk. Even if we assume that the concurrent crystallization of the film did not have a significant impact on the result of the self-diffusivity measurements, the nanoscale dimensions of the ice samples used in these experiments still raise questions about the influence of confinement on the transport phenomena. Indeed, as we already mentioned, the diffusivity of water in crystalline ice films of similar microscopic dimensions appears to be greater than that in the bulk single crystal ice.[31]

Recently, Bhat *et al.* reported the electron spin resonance (ESR) spectra of 4-hydroxy-TEMPO in *doped* ASW obtained by flash freezing of water samples in glass capillaries.[35] From the analysis of the ESR spectra of 4-hydroxy TEMPO trapped in ASW, they concluded that the glass transition of pure ASW must occur at approximately 135 K. Thus, once again, the influence of the impurities on the glass transition comes into consideration. Indeed, as noted by the authors, the spin probe ESR technique is sensitive to the "weakly" associated water, which forms a small fraction of the entire sample, i.e., to the water in the immediate vicinity of the ESR probe species (4-hydroxy TEMPO). While we do not question the possible existence of the glass transition in such confined aqueous system at 135 K, we point out that the results of these experiments may not be automatically extended to the case of *pure macroscopic* ASW.

Finally, we consider experiments where a blunted conical indentor was used to measure deformation of pressure-amorphized ice.[36] These studies showed that ASW prepared from annealing of high density amorphous ice softened significantly at approximately 142 K Based on this observation, it was concluded that ASW behaved as a viscous liquid under this conditions, i.e., that the glass transition in ASW must occur at temperatures below 143 K. Although the experiments cited above were conducted with macroscopic ASW samples, we argue that the observed deformation of the amorphous solid may be still driven by interfacial phenomena and, therefore, may not be representative of properties of bulk ASW phase. Indeed, a tungsten wire can slice rather rapidly through crystalline ice samples at temperatures several degrees below bulk melting point. However, the velocity of the wire is determined not by the properties of the bulk crystalline phase but by the *thickness* of the quisiliquid layer formed at the wire-ice interface.[37] Thus, it is unclear if the observed sinking of the steel indentor into ASW at temperatures near 142 K is due to sudden changes in *bulk* properties of ASW sample and not due to variations in the properties of thin layer of confined ASW near the indentor surface.

IV. SUMMARY AND CONCLUSIONS

Results of ultrafast microcalorimetry studies reported in this article provide evidence that the presence of impurities may have a dramatic effect on molecular kinetics in ASW at low temperature. We argue that this may be due to perturbation of the hydrogen bond network of ASW. Therefore, the results of the experiments conducted with ASW samples, which contained impurities or were confined to nanoscale dimensions, must be interpreted with caution. In contrast to previous studies, the ultrafast microcalorimetry results reported here indicate that the glass transition in ASW may occur at temperatures significantly higher than claimed in some of the past studies. Therefore, the result of our studies support the hypothesis that water, in fact, may exhibit anomalous crossover from fragile to strong nature while going from moderately supercooled region to deeply supercooled region. In short, the properties of ASW are far from being completely understood and that more experiments are needed to gain insights into the relationships between various noncrystalline forms of H_2O.

[1] For a review, see O. Mishima and H. Stanley, Nature (London) **396**, 329 (1998).
[2] R. J. Speedy, J. Phys. Chem. **86**, 982 (1982).
[3] H. E. Stanley and J. Teixeira, J. Chem. Phys. **73**, 3404 (1980).
[4] For a review, see R. A. Baragiola, in *Water in Confining Geometries*, Springer Series in Cluster Physics, edited by V. Buch and J. P. Devlin (Springer-Verlag, Berlin, 2003), pp. 359–395.
[5] P. BruEggeller and E. Mayer, Nature (London) **288**, 569 (1980).
[6] J. Dubochet and W. A. McDowall, J. Microsc. **124**, RP3 (1981).
[7] J. Huang and L. S. Bartell, J. Phys. Chem. **99**, 3924 (1995).
[8] L. S. Bartell and J. Huang, J. Phys. Chem. **98**, 7455 (1994).
[9] L. S. Bartell and Y. G. Chushak, in *Water in Confining Geometries*, Springer Series in Cluster Physics, edited by V. Buch and J. P. Devlin (Springer-Verlag, Berlin, 2003), pp. 399–424.
[10] G. P. Johari, A. Hallbrucker, and E. Mayer, Nature (London) **330**, 552 (1987).
[11] A. Hallbrucker, E. Mayer, and G. P. Johari, Philos. Mag. B **60**, 179 (1989).
[12] For example, see R. S. Smith, Z. Dohnalek, G. A. Kimmel, K. P. Stevenson, and B. D. Kay, Chem. Phys. **258**, 291 (2000).
[13] R. S. Smith, C. Huang, E. K. L. Wong, and B. D. Kay, Surf. Sci. Lett. **367**, L13 (1996).
[14] R. S. Smith and B. D. Kay, Surf. Rev. Lett. **4**, L13 (1996).
[15] V. Sadtchenko, M. Brindza, M. Chonde, B. Palmore, and R. Eom, J. Chem. Phys. **121**, 11980 (2004).
[16] C. A. Angell, Chem. Rev. (Washington, D.C.) **102**, 2627 (2002).
[17] V. Velikov, S. Borick, and C. A. Angell, Science **294**, 2335 (2001).
[18] C. Alba, L. E. Busse, D. J. List, and C. A. Angell, J. Chem. Phys. **92**, 617 (1990).
[19] A. Dob, G. Hinze, B. Schiener, J. Hemberger, and R. Bohmer, J. Chem. Phys. **107**, 1740 (1997) and references therein.
[20] Y. P. Handa, O. Mishima, and E. Whalley, J. Chem. Phys. **84**, 2766 (1986).
[21] G. P. Johari, G. Fleissner, A. Hallbrucker, and E. Mayer, J. Phys. Chem. **98**, 4719 (1994).
[22] G. P. Johari, J. Chem. Phys. **105**, 7079 (1996).

[23] R. C. Smith, C. Huang, and B. D. Kay, J. Phys. Chem. B **101**, 6123 (1997).
[24] K. Ito, C. T. Moynihan, and C. A. Angell, Nature (London) **398**, 492 (1999).
[25] P. G. Debenedetti, J. Phys.: Condens. Matter **15**, R1669 (2003).
[26] J. G. Dash, B. L. Mason, and J. S. Wettlaufer, J. Geophys. Res. **106**, 20395 (2001).
[27] J. G. Dash, H. Y. Fu, and J. S. Wettlaufer, Rep. Prog. Phys. **58**, 115 (1995).
[28] J. S. Wettlaufer, Philos. Trans. R. Soc. London, Ser. A **357**, 3403 (1999).
[29] V. Sadtchenko and G. E. Ewing, J. Chem. Phys. **116**, 4686 (2002) and references therein.
[30] For a review, see J. P. Devlin and V. Buch, in *Water in Confining Geometries*, Springer Series in Cluster Physics, edited by V. Buch and J. P. Devlin (Springer-Verlag, Berlin, 2003), pp. 426–462.
[31] F. E. Livingston and S. M. George, J. Phys. Chem. A **102**, 10280 (1998).
[32] J. S. Wettlaufer, Phys. Rev. Lett. **82**, 2516 (1999).
[33] J. P. Devlin, Int. Rev. Phys. Chem. **9**, 29 (1990).
[34] H. Tanaka and K. Koga, in *Water in Confining Geometries*, Springer Series in Cluster Physics, edited by V. Buch and J. P. Devlin (Springer-Verlag, Berlin, 2003), pp. 152–177.
[35] S. N. Bhat, A. Sharma, and S. V. Bhat, Phys. Rev. Lett. **95**, 235702 (2005).
[36] G. P. Johari, J. Phys. Chem. B **102**, 4711 (1998).
[37] R. R. Gilpin, J. Colloid Interface Sci. **77**, 435 (1980).